Journal of the European Ceramic Society 22 (2002) 1959–1969

www.elsevier.com/locate/jeurceramsoc

Hot corrosion of cordierite/mullite composites by Na-salts

Junichi Takahashi*, Yoshie Kawai, Shiro Shimada

Division of Materials Science and Engineering, Graduate School of Engineering, Hokkaido University, N-13 W-8 Kita-ku, Sapporo 060-8628, Japan

Received 21 March 2001; received in revised form 29 November 2001; accepted 8 December 2001

Abstract

Cordierite/mullite (C/M) ceramic composites were corroded by NaCl and Na_2SO_4 at 1000 °C for 24 h. The predominant corrosion products in attack by the Na-salts were found to be nepheline and carnegieite for the cordierite and mullite component, respectively. NaCl attacked both components with different corrosion rates, producing corrosion layers consisting of two distinct regions where both cordierite and mullite were chemically attacked near the surface region and only the cordierite phase was damaged in the succeeding inner part. In the hot corrosion by Na_2SO_4, on the other hand, only the cordierite component was severely attacked in the composites, resulting in occurrence of selective corrosion. Thus, the corrosion of the C/M composites by the Na-salts proceeded through the path of the less resistive cordierite component at 1000 °C in air.

Keywords: Composites; Cordierite; Corrosion; Molten salts; Microstructure; Mullite

1. Introduction

Cordierite ($Mg_2Al_4Si_5O_{18}$) ceramics show several superior high temperature properties such as excellent thermal shock resistance and chemical stability at elevated temperatures. Especially, the superior thermal shock resistance property enables them to be applied as the filter element of advanced power generation systems.[1–3] However, the relatively poor structural durability of the cordierite ceramics should be improved for reliable long-term filter operation. A possible method for fulfilling this requirement is to add a reinforcing phase and fabricate a ceramic composite. Because mullite ($Al_6Si_2O_{13}$) ceramics have a high melting temperature, good resistance against creep deformation, and a moderate thermal expansion coefficient, the combination of cordierite with mullite (i.e. the C/M composite) would provide an advanced filter element with less degradation of thermal shock resistance property. Additionally, the elongated mullite grains can be formed by the employment of an appropriate fabrication procedure,[4–9] which may cause improved mechanical properties in the resulting C/M composite ceramics.

For the practical usage of filter elements in a combustion environment, it is very important to elucidate their corrosion behavior at elevated temperatures. The present authors have already reported the hot corrosion of the cordierite ceramics attacked by NaCl, Na_2SO_4, KCl and K_2SO_4.[10] For alumina–silica compositions including mullite, corrosion by Na and K salts was studied under different conditions and the results were examined on the basis of the Na_2O–Al_2O_3–SiO_2 phase diagram.[11–14] Compared with the extensive examinations on the interaction of the corrosive species and cordierite or mullite ceramics, there is little information on the hot corrosion of C/M composites. In the present study, C/M composite bodies with different C/M ratios, which consisted of elongated mullite grains, were fabricated from the corresponding mixtures of alumina and silica sols and $Mg(OH)_2$ powder. These ceramic composites were heated in a concentrated NaCl or Na_2SO_4 atmosphere at 1000 °C for 24 h and the corrosion characteristic was examined for the C/M composite system.

2. Experimental procedure

2.1. Fabrication and characterization of C/M composites

The C/M composites examined in this study were those with molar ratios of C:M = 8:2, 5:5 and 2:8 (hereafter they are abbreviated as C80, C50 and C20, respectively). Starting materials used were commercially available chemicals; alumina and silica sols (both from

* Corresponding author. Tel./fax: +81-11-706-6572.
E-mail address: tkjun@eng.hokudai.ac.jp (J. Takahashi).

0955-2219/02/$ - see front matter
PII: S0955-2219(01)00529-5

Nissan Kagaku) and $Mg(OH)_2$ powder (Kojundo Kagaku). Required amounts of the corresponding materials were weighed and treated in a following procedure to obtain each starting powder having a fixed C:M composition. At first, both sols were well stirred and then a $Mg(OH)_2$ powder suspended in distilled water was poured in the mixed sol. After adding an appropriate amount of distilled water to adjust the viscosity of a slurry, they were thoroughly mixed for several hours. In the successive microwave drying process, most of water contained in the slurry was removed to produce a dried gel. The gel was ground and calcined at 1300 °C for 4 h, which was followed by ball milling to obtain a fine powder for sintering. Green compacts formed by uniaxial and isostatic pressing were sintered in the temperature range 1445–1450 °C for 10 h. Sintered density was measured by Archimedes method and the solid phases formed after calcination and sintering were identified by XRD (X-ray powder diffractometry). Mullite ceramics were fabricated in the same procedure except for calcining and sintering temperatures of 1100 and 1600 °C, respectively.

Composite samples thus obtained were characterized by microstructural observation and thermal expansion property. Typical microstructure of the sintered C/M composites are shown in Fig. 1, in which secondary electron images [SEI, (a), (c), (e)] and backscattered electron images [BSE, (b), (d), (f)] are given. Elongated mullite grains, which were expected to improve the mechanical properties of the composites, can be seen in all the samples fabricated. For the C20 composite [Fig. 1(f)], a limited number of large mullite grains with large aspect ratios existed in addition to a large number of very small ones. Measured relative density of each composite was 94.1, 92.8 and 90.8% for the C80, C50 and C20 samples, respectively. It was also evident that there were comparatively large pores in the C80 and C50 composites. The thermal expansion coefficients of the composite samples linearly changed with the C/M ratio from 9.5×10^{-7}/K for C100 (cordierite ceramics) to 4.0×10^{-6}/K for C0 (mullite ceramics).

2.2. Hot corrosion

NaCl (mp 801 °C) and Na_2SO_4 (mp 884 °C) were used as sources of corrosive species of sodium, chlorine and sulfur. Interaction of sintered composites and each corrosive chemical reagent was conducted in an covered alumina crucible in which a composite sample was placed on a Pt-box with a surrounding powder bed of a corrosive chemical. After each corrosion experiment, the as-corroded sample was washed with distilled water to dissolve solid materials deposited on the surface (NaCl or Na_2SO_4). The outmost surface of each corroded sample was characterized by XRD (X-ray diffractometry) and SEM (scanning electron microscopy) attached with EDS (energy dispersive X-ray spectroscopy) for the identification of the solid phases formed and observation of morphological change of the corroded surface. The distributions of specified elements in a cross-sectional area of a corroded sample were analyzed with WDS (wavelength dispersive X-ray spectroscopy). Further experimental details can be seen in the previous study.[10]

3. Results and discussion

3.1. Base studies on hot corrosion of cordierite and mullite ceramics by Na-salts

Prior to the hot corrosion of the C/M composites, the individual corrosion behavior of the cordierite and mullite ceramics was summarized.

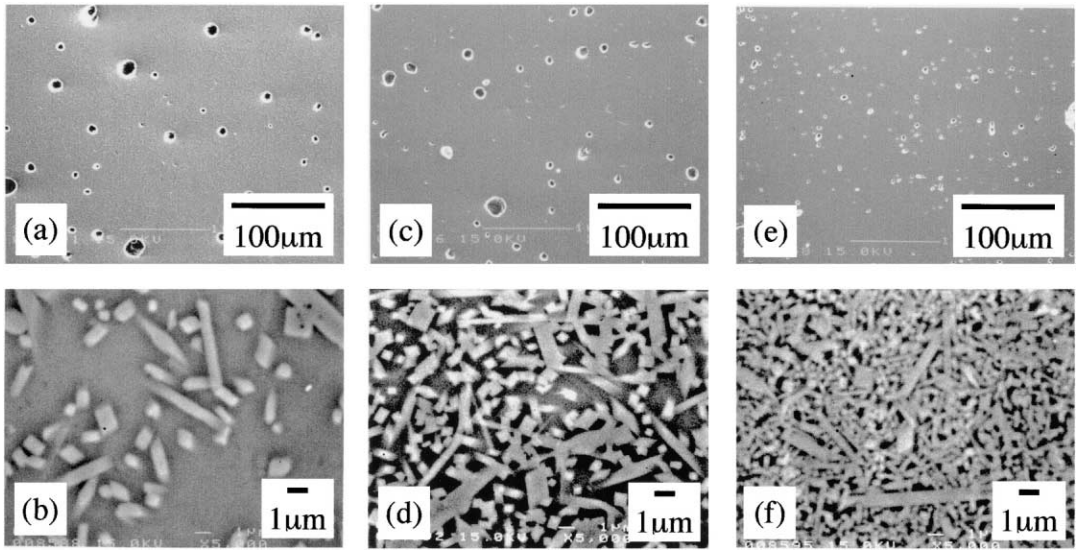

Fig. 1. Microstructures of composites; (a) C80 (SEI), (b) C80 (BSE), (c) C50 (SEI), (d) C50 (BSE), (e) C20 (SEI) and (f) C20 (BSE).

The cordierite ceramics were corroded by Na_2SO_4 at 1000 °C under a flowing oxygen environment.[1] In the first hour of the corrosive reaction, a solidified Na_2SO_4 layer was observed on the corroded surface. As the reaction continued, Mg_2SiO_4 crystallites could be clearly seen for the sample heated for 24 h. After 72 h of reaction, X-ray dot maps of the polished cross-section indicated that the corrosion layer consisted of the larger $NaAlSiO_4$ grains with an upper layer of Mg_2SiO_4. From XRD analysis and microstructural observation of the corroded samples, the overall reaction was suggested as follows:

$$2Na_2SO_4(l) + Mg_2Al_4Si_5O_{18}(s) \rightarrow 4NaAlSiO_4(s) + Mg_2SiO_4(s) + 2SO_2(g) + O_2(g) \quad (1)$$

The hot corrosion of cordierite ceramics by NaCl and Na_2SO_4 was also conducted in an alumina crucible in the temperature range from 700 to 1200 °C.[10] In case of NaCl attack, the corrosion products at 1000 °C for 4 h were identified with MgO, α-Al_2O_3 and a considerable amount of nepheline ($NaAlSiO_4$). The thickness of the corroded region was estimated to be about 8 and 20 μm for the samples heated for 4 and 24 h, respectively. The surface of the latter was characterized with a number of small idiomorphic MgO crystals. By the cross-sectional WDX analysis, a Mg-enriched outer surface layer was followed by a Mg-missing but Na-penetrating region. The similar distribution map of the Mg and Na elements was observed for the cordierite ceramics attacked by Na_2SO_4 at 1000 °C for 24 h, the surface of which was covered with plate-like Mg_2SiO_4 (forsterite) particles. Since XRD results of the corroded samples showed small peaks of nepheline and cristobalite, the hot corrosion by Na_2SO_4 less proceeded than NaCl attack under the same experimental conditions.

Jacobson et al. studied corrosion of mullite ceramics by molten salts of different Na_2O activities.[14] The Na_2O activity was set by using thin films of Na_2CO_3 and Na_2SO_4 and the corresponding overpressure of $CO_2(g)$ and $SO_3(g)$. The corrosion product was Al_2O_3 in a lower activity of $a_{Na_2O} = 3.6\times10^{-12}$ (acidic molten salt) at 1000 °C. With an increasing Na_2O activity (more-basic molten salts), various Na_2O–Al_2O_3–SiO_2 compounds were additionally produced. After 24 h of reaction in the activity of 8.1×10^{-7} (at 1000 °C), a product layer ~15 μm thick formed and the composition of the product was determined to be Na_2O–Al_2O_3–SiO_2.

The following are the results of the hot corrosion of mullite ceramics by NaCl and Na_2SO_4 obtained in the present study. Fig. 2 shows XRD patterns of corroded surfaces of mullite ceramics by NaCl at 1000 and 1200 °C. Small peaks of carnegieite appeared after heating at 1000 °C for 4 h, and gradually intensified with prolonged heating. Mullite peaks on the surface almost disappeared in a sample heated at 1000 °C for 24 h, indicating the progression of the corrosion by NaCl. The depth of Na penetration in the bulk samples corroded for 24 h was evaluated to be about 10 μm from the cross-sectional Na map given in Fig. 3(a). As clearly seen in Fig. 2(e), the hot corrosion of mullite ceramics by NaCl was remarkably enhanced at 1200 °C, in which the corrosion layer with more than 20 μm in thickness [Fig. 3(b)] was found to be composed of several solid phases of carnegieite, β-alumina, nepheline etc. When the mullite sample was attacked by Na_2SO_4, on the other hand, only the carnegieite phase was detected as corrosion product. The intensities of the carnegieite peaks were very weak after corrosion at 1000 °C for 24 h. However, enhanced corrosion was observed after attack by Na_2SO_4 at 1200 °C.

$NaAlSiO_4$, which was formed as the corrosion product in the present study, shows four types of modification. The low temperature α-nepheline (hexagonal) transforms to the β-nepheline (orthorhombic) at 900 °C and successively to β-carnegieite (cubic) at 1250 °C.[15,16] When a derivative such as $NaAlO_2$ coexists, solid solutions of $Na_yAl_ySi_{1-y}O_2$ ($0.5 \leqslant y \leqslant 1$) can be formed between $NaAlO_2$ and $NaAlSiO_4$. The incorporation of $NaAlO_2$ into carnegieite can stabilize the high temperature form. On cooling, the stabilized β-carnegieite transforms at a substantially lowered temperature of 687 °C to α-carnegieite. This phase relation explained the different crystalline phases of $NaAlSiO_4$ observed for the hot corrosion of the cordierite (nepheline) and mullite (carnegieite) ceramics. The basic corrosion reactions

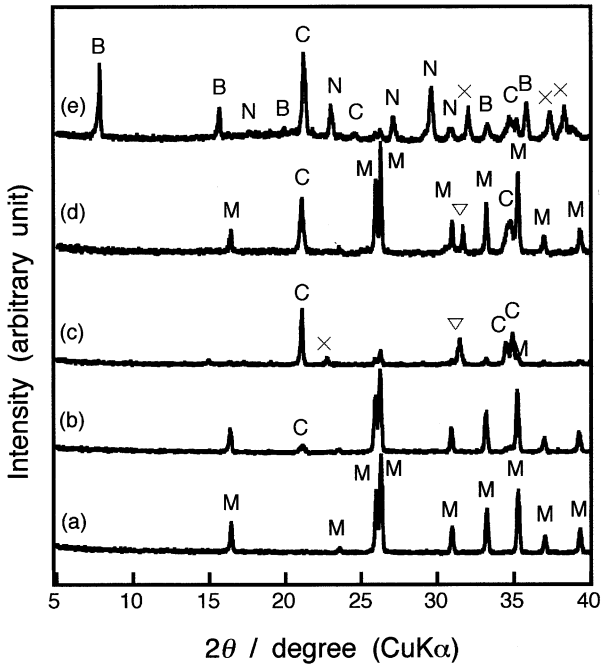

Fig. 2. XRD patterns of (a) as-sintered mullite and mullite ceramics corroded by NaCl at 1000 °C for (b) 4 h and (c) 24 h, and at 1200 °C for (d) 4 h and (e) 24 h. (M: mullite, C: carnegieite, N: nepheline, B: Na-β-alumina, ▽: NaCl and X: unknown.)

occurring between the host ceramics and corrosive NaCl at 1000 °C are as follows:

for cordierite

$$Mg_2Al_4Si_5O_{18}(s) + 4NaCl(l) + O_2(g) \rightarrow 4NaAlSiO_4(s) + SiO_2(s) + 2MgO(s) + 2Cl_2(g) \quad (2)$$

for mullite

$$2Al_6Si_2O_{13}(s) + 8NaCl(l) + O_2(g) \rightarrow 4NaAlSiO_4(s) + 4Al_2O_3(s) + 2Na_2O(s) + 4Cl_2(g) \quad (3)$$

$$Al_2O_3(s) + Na_2O(s) \rightarrow 2NaAlO_2(s) \quad (4)$$

It is definitely evident that the stabilized β-carnegieite is formed in the hot corrosion of mullite, although no $NaAlO_2$ phase was detected by XRD analysis.

3.2. Corrosion behavior of C/M composites at 1000 °C

3.2.1. Attack by NaCl

XRD profiles of the composite surfaces corroded by NaCl at 1000 °C for 24 h are revealed in Fig. 4. The diffraction pattern of the C80 sample is very similar to that of cordierite, with the major corrosion products of cristobalite (marked by Cr in Fig. 4), nepheline (N) and MgO (P). For the C50 composite, carnegieite (C) can be additionally detected with an decreasing intensity of nepheline. The C20 and mullite samples show relatively simple XRD profiles in which only carnegieite appears as the corrosion product.

Figs. 5 and 6 show the results of X-ray elemental analysis conducted for the polished cross-sections of the C80 and C20 composites, respectively. As can be seen in the Mg map in Fig. 5, the corroded region of the C80

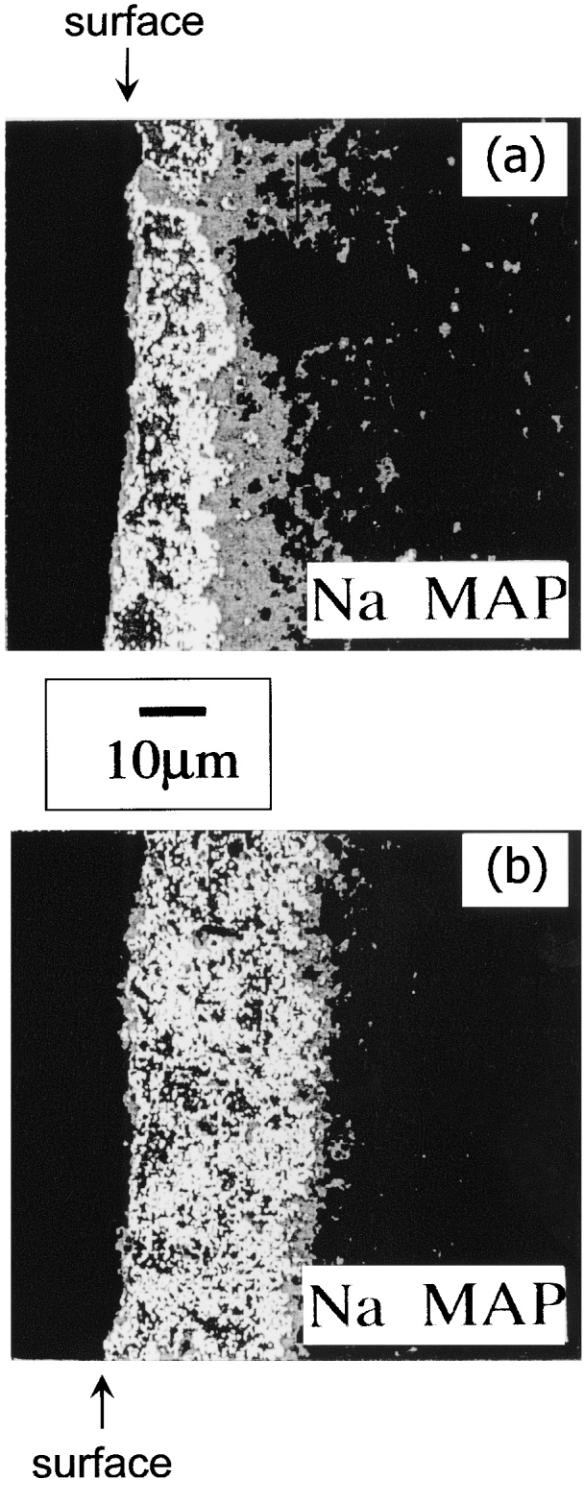

Fig. 3. Na dot maps of polished cross-section of mullite samples corroded by NaCl for 24 h at (a) 1000 °C and (b) 1200 °C.

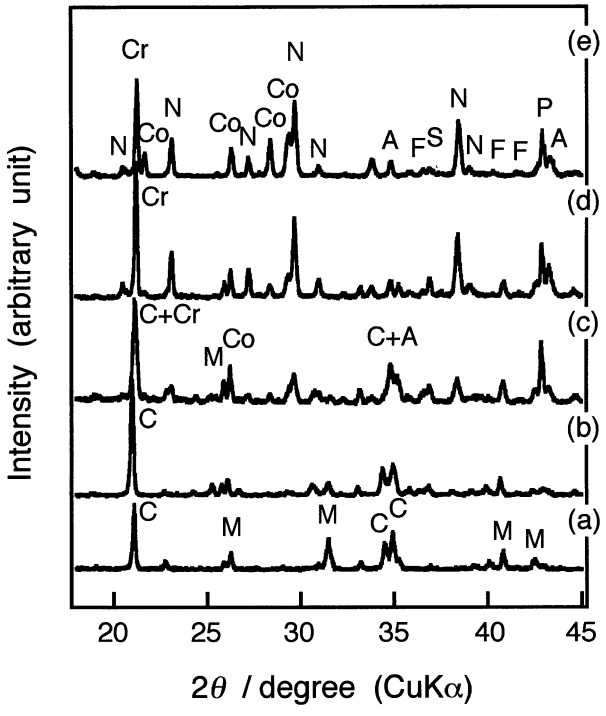

Fig. 4. XRD patterns of (a) mullite, (b) C20, (c) C50, (d) C80 and (e) cordierite samples attacked by NaCl at 1000 °C for 24 h. (Co: cordierite, M: mullite, C: carnegieite, N: nepheline, Cr: cristobalite, P: MgO, A: α-alumina, S: spinel and F: forsterite.)

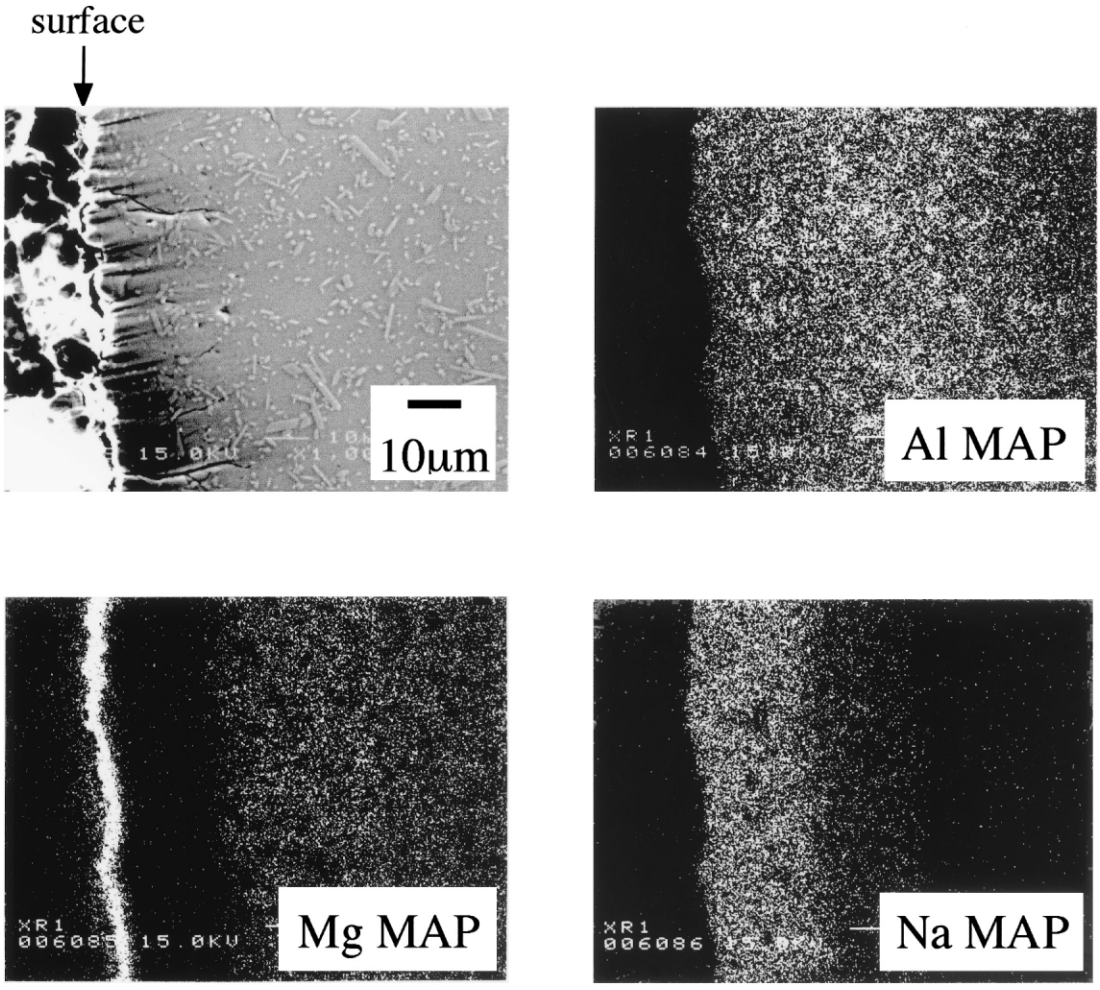

Fig. 5. SEM image (SEI) and X-ray elemental dot maps for polished cross-section of C80 composite corroded by NaCl.

composite consisted of an outmost surface layer with a high Mg concentration (corresponding to MgO), which was abruptly followed by the Mg-deficient part. The corrosive Na species clearly penetrated into the composite body and distributed uniformly until the Mg element could be detected with an appreciable level again. The depth of the Na penetration corresponded to the Mg-deficient region. Accordingly, the thickness of the corroded region was estimated to be about 20–25 μm for the C80 composite. This characteristic Mg distribution was also observed in the hot corrosion of the cordierite ceramics by NaCl.[10] In addition, the Na penetration similarly extended to about 20 μm depth from the sample surface at 1000 °C for 24 h.

On the contrary, somewhat different X-ray elemental maps are shown for the C20 sample in Fig. 6. (In Figs. 6 and 9, the Mg signals of the C20 sample were enhanced using a software package.) The segregation of Mg on the outmost surface was less than that of the C80 sample, which was due to the smaller content of the cordierite phase. However, the Mg-deficient region considerably extended into inner part of the sample (ca. 40 μm from the surface). Additionally, the Na map revealed that there was a boundary from which the Na concentration substantially changed. The Na-enriched region extended up to 20 μm from the surface, which was followed by the region with a very low Na concentration through the Mg-deficient part. The Al and Si maps similarly consisted of two parts with the correspondingly different concentrations. The BSE (COMPO image) in Fig. 6 shows that the composition of the Na-enriched region is definitely different from that of the Na-poor part. Probably, both the cordierite and mullite phases were severely corroded in the Na-enriched region whereas only the minor cordierite component was attacked in the inner Na-poor part. The schematic presentation of this situation can be seen in Fig. 7.

Comparing the Na distributions between Figs. 5 (C80) and 6 (C20), the C80 composite showed homogeneous distribution of the Na element through the Mg-dificient region. This might be explained by the mullite content in the composite. Because it was much smaller for the C80 composite than for the C20 one and additionally cordierite shows less corrosion resistance

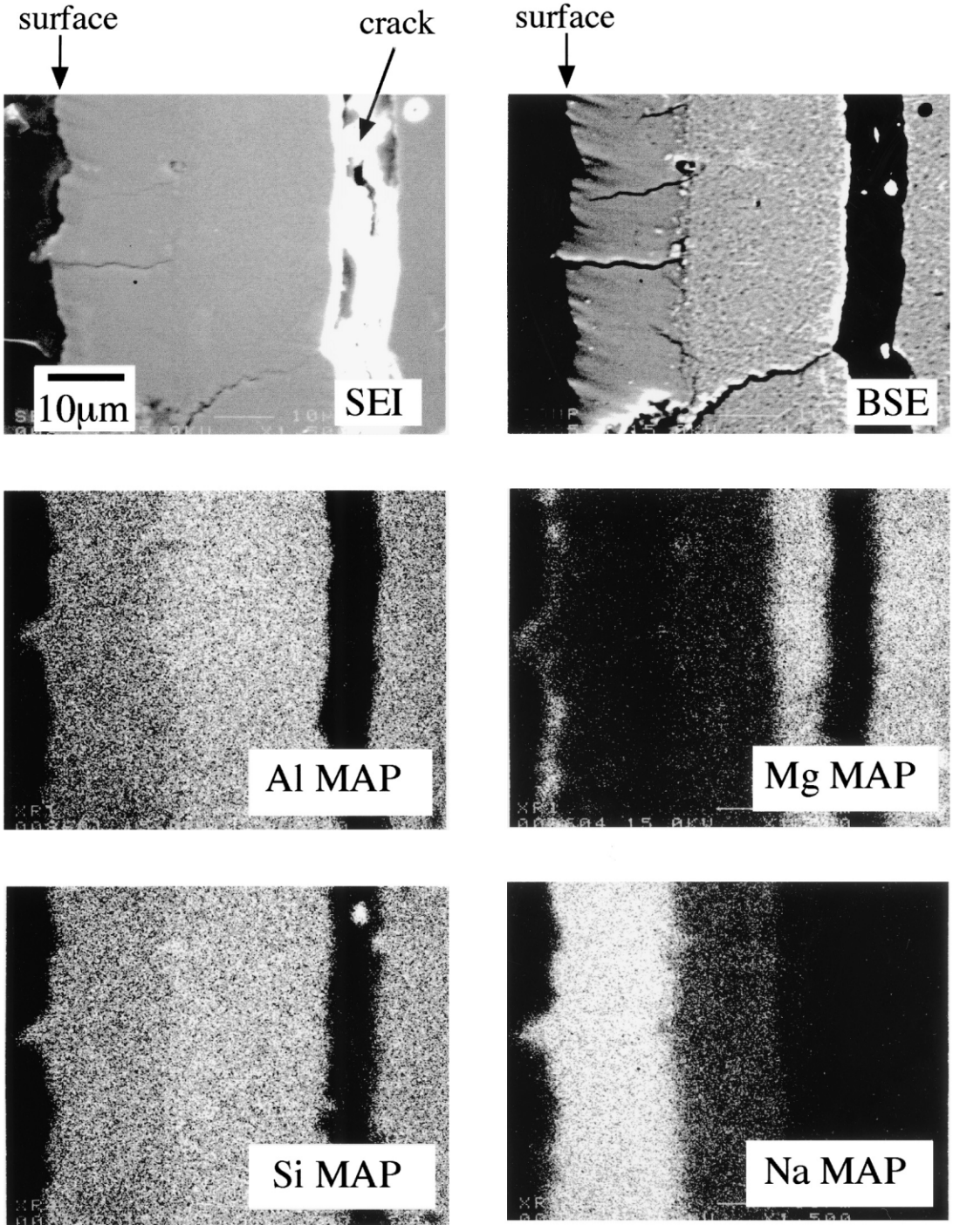

Fig. 6. SEM images and X-ray elemental dot maps of C20 composite corroded by NaCl.

against NaCl attack than mullite (Fig. 4), selective corrosion would be emphasized for the C20 composite. The occurrence of selective corrosion in the C80 composite was supported by the microstructure of the corrosion layer where elongated mullite grains could be still observed in inner part (Fig. 5). Thus based on the Mg and Na maps, the thickness of the corrosion layer could be estimated to be about 40 μm for the C20 sample, which was considerably larger than that of the C80 composite. Sintering temperature employed in fabricating the C/M composites in this study was determined to be 1445–1450 °C at which fully densified cordierite ceramics was obtainable without decomposition of the cordierite phase. However, for the mullite particles, substantial neck growth between particles hardly occurs at the temperature range. The extremely different densification characteristics between the cordierite and mullite components caused the lowering in the sintered

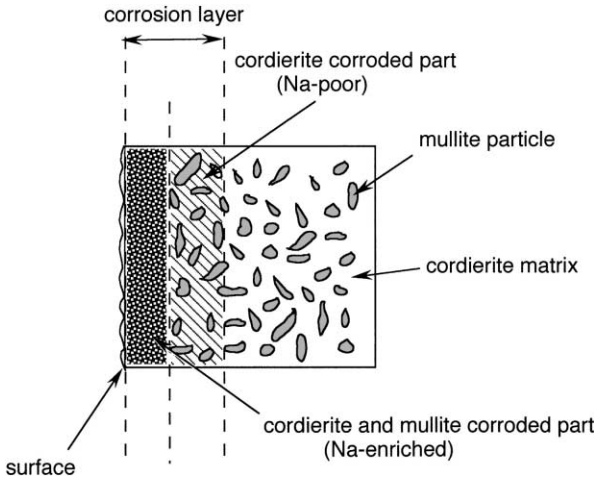

Fig. 7. Schematic presentation of cross-section of C/M composite attacked by NaCl.

density of the C20 composite. In addition to the visible pores in micrometer size, it should definitely contain a lot of invisible unconnected areas between mullite particles. These invisible voids served as penetration routes of corrosive species more deeply into the interior of the corroded sample. Thus the specified sintering character of the C20 composite may be responsible for the extended corrosion by NaCl.

3.2.2. Attack by Na_2SO_4

Fig. 8 shows XRD results of composite surfaces corroded by Na_2SO_4 at 1000 °C for 24 h. The corrosion products of the C80 and C50 composites were basically similar to those detected in the chemical attack by NaCl. This result definitely indicated that the cordierite component was severely corroded by both NaCl and Na_2SO_4 at 1000 °C. However, substantially different corrosion behavior was observed in the C20 composite between NaCl and Na_2SO_4 attacks. Intensified mullite peaks are clearly seen in the XRD pattern of the C20 sample corroded by Na_2SO_4, suggesting that mullite showed superior resistance against Na_2SO_4 attack at 1000 °C. Besides, XRD peaks of nepheline detected in the C20 composite clearly indicated that only the cordierite component was corroded by Na_2SO_4 at 1000C in C/M composites, because the chemical attack by Na-salts in air for cordierite and mullite ceramics caused the formation of nepheline and carnegieite as the predominant corrosion product, respectively. Therefore it was concluded that the mullite component possessed better corrosion resistance against Na_2SO_4 than cordierite at 1000 °C.

Cross-sectional Mg and Na maps are revealed in Fig. 9 for the corroded C80 and C20 samples. In the hot corrosion by Na_2SO_4, the Mg-enriched surface layer and successive Mg-deficient region can be similarly observed in both composites. This characteristic distribution of the Mg element was necessarily observed in the cordierite-

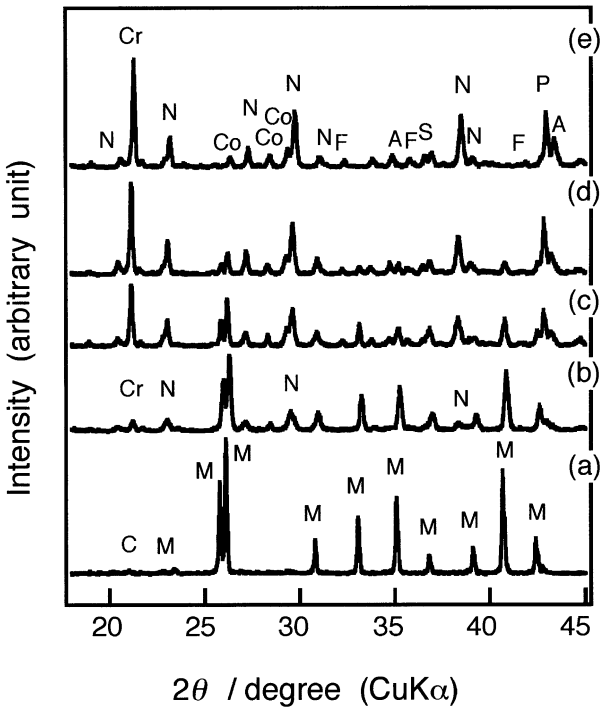

Fig. 8. XRD patterns of (a) mullite, (b) C20, (c) C50, (d) C80 and (e) cordierite samples corroded by Na_2SO_4 at 1000 °C for 24 h. (Notations are the same as those in Fig. 4.)

containing materials corroded by Na-salts under conditions examined in this study. Concerning the Na map of the C20 sample, it should be noted that the corrosive Na species homogeneously distributed through the corroded region. These results substantially different from those obtained in the hot corrosion of C20 sample by NaCl, in which the Na map consisted of two distinctive parts corresponding to the severe corrosion of both components and the selective corrosion of the cordierite component, respectively. The homogeneous Na distribution in the C20 sample (Fig. 9) supported the occurrence of the selective corrosion of the cordierite phase in the C/M composites by Na_2SO_4 attack. Therefore, in the C20 composite containing cordierite as a minor phase, only the cordierite component was predominantly and seriously attacked by Na_2SO_4 to form nepheline as corrosion product. For all the composites corroded in the present study, no appreciable amount of chlorine nor sulfur was detected by X-ray elemental analysis.

3.2.3. Mg compounds formed on the corroded surfaces

Figs. 10 and 11 show the surface morphology of the composites corroded by NaCl and Na_2SO_4, respectively, with the associated EDS results of the marked particles (or regions). In case of NaCl attack, idiomorphic MgO particles were predominantly observed for the C80 composite, which was consistent with the XRD result. The growth of idiomorphic MgO particles associated with the characteristic Mg distribution in the corroded

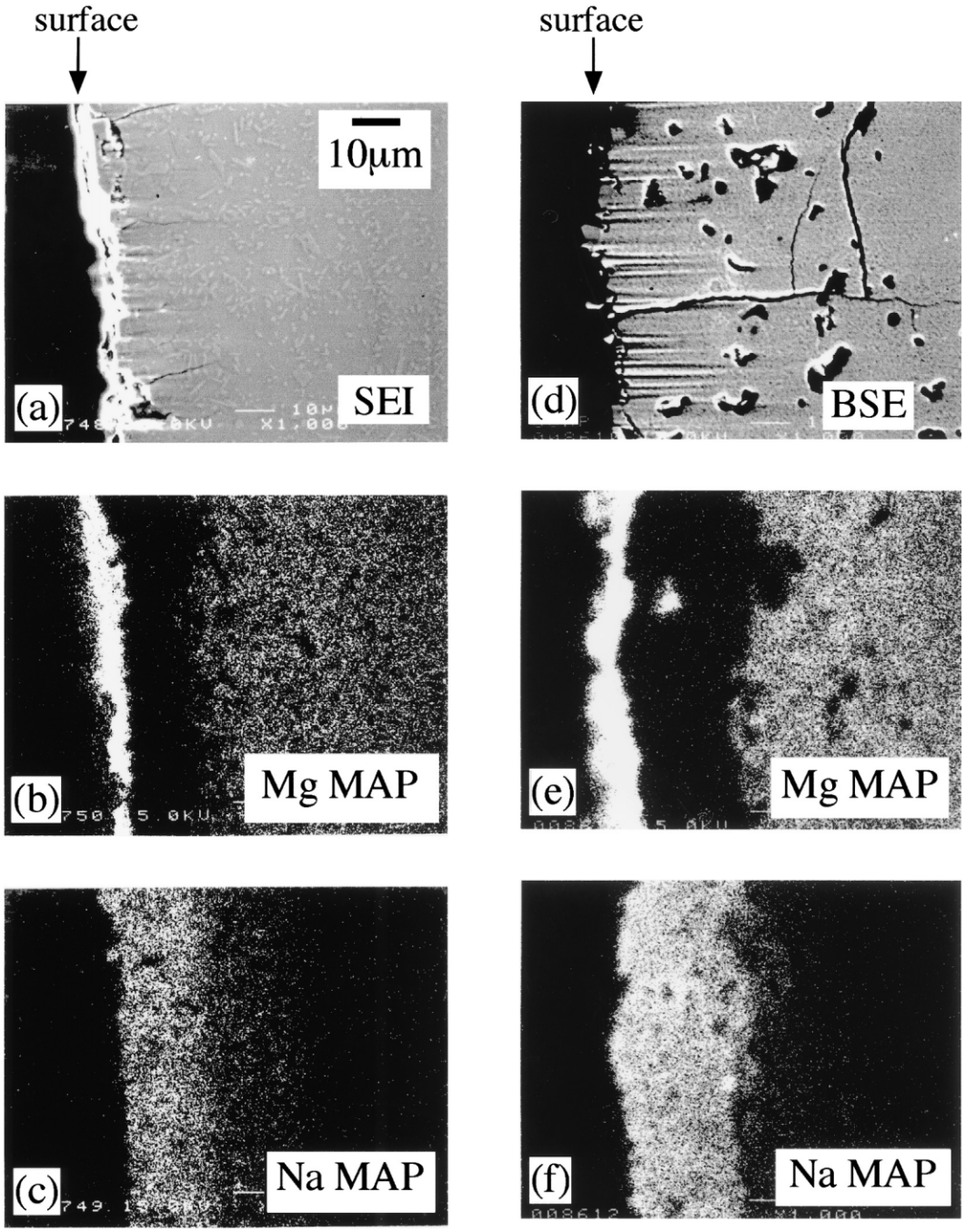

Fig. 9. Cross-sectional Mg and Na dot maps for (a) to (c) C80 and (d) to (f) C20 composites attacked by Na_2SO_4.

region (Fig. 5) might be explained by some mechanism by which Mg-related species should be transported up to the surface of a corroded composite. Possible reactions occurring at corrosion front were

$$Mg_2Al_4Si_5O_{18}(s) + 4NaCl(l) \rightarrow 4NaAlSiO_4(s) + SiO_2(s) + 2MgCl_2(l) \quad (5)$$

$$Mg_2Al_4Si_5O_{18}(s) + 4NaCl(l) + O_2(g) \rightarrow 4NaAlSiO_4(s) + SiO_2(s) + 2MgO(s) + 2Cl_2(g) \quad (6)$$

Using reported data,[17,18] the free energy change of each reaction at 1000 °C was calculated to be −425 and−443 kJ for the reaction (5) and (6), respectively. It was obvious that each of these reactions thermodynamically proceeded at 1000 °C. If the $MgCl_2$ species were substantially formed as a result of NaCl attack, it was likely for a number of the $MgCl_2$ molecule to diffuse towards the sample surface as vapor phase (vapor pressure of $MgCl_2$ is 2.6 kPa at 988 °C) or soluble species in the corrosive NaCl melt (eutectic temp. is 450 °C at 48 mol.% $MgCl_2$ in the system NaCl–$MgCl_2$).[19] On

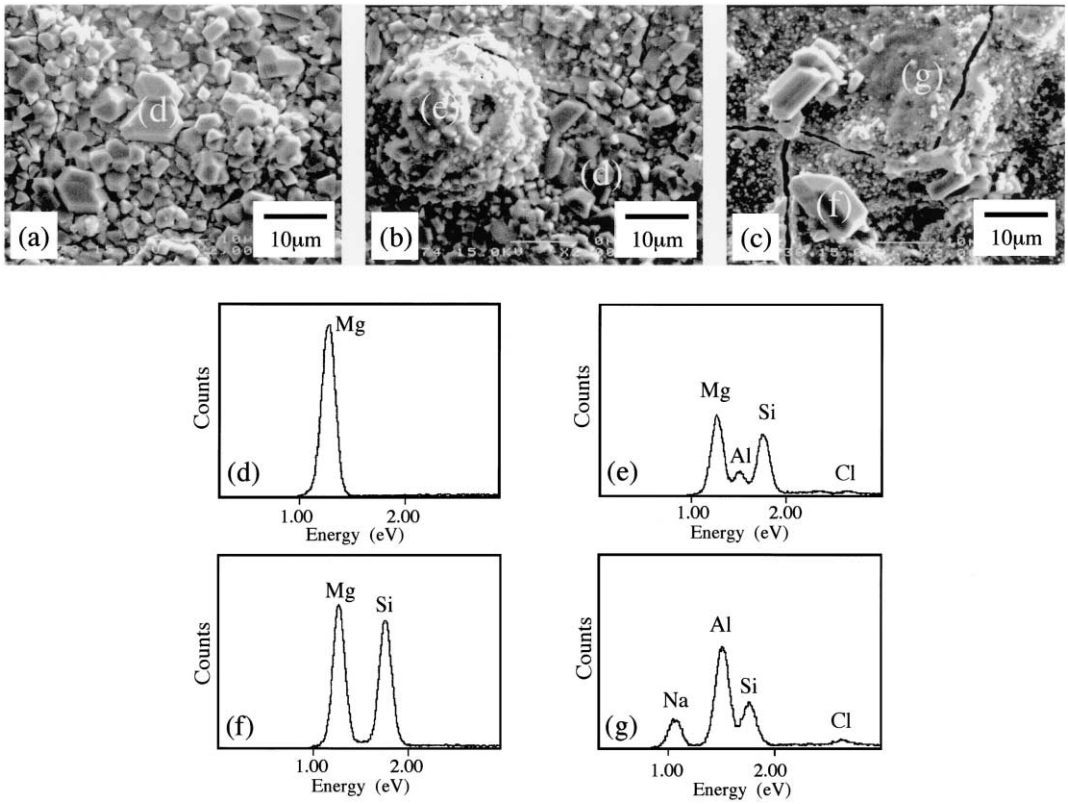

Fig. 10. Surface morphologies of (a) C80, (b) C50, (c) C20 composites corroded by NaCl with EDS results of (d), (e), (f) particles and (g) region.

the outmost surface, the $MgCl_2$ species reacted with oxygen to produce the MgO particles. Alternatively, the formation of the MgO species [Eq. (6)] might also be one of the possible reactions in the NaCl attack. Concerning the diffusion of the MgO species up to the outer surface, however, transportation of the MgO species either as gas phase or soluble species hardly occurred because of its very low vapor pressure (about 1×10^{-6} Pa at 1400 °C in $PO_2=20$ kPa[20]) and a very limited solubility of MgO in molten NaCl (the solubility of MgO in molten NaCl is 0.0010 mol.% at 1000 °C[21]). Therefore, the formation of $MgCl_2$ based on Eq. (5) and the successive diffusion of the species up to the outer surface would be a favorable process in case of NaCl attack at 1000 °C.

In the C20 sample showing very strong XRD peaks of carnegieite [Fig. 4(b)], relatively large idiomorphic particles of forsterite were detected [designated by (f) in Fig. 10]. Since this composite contained a smaller amount of the cordierite component, the number of the $MgCl_2$ species formed was reduced. Under this chemical environment, the following reaction might preferably take place because a corrosion product, $SiO_2(s)$, should provide reaction site.

$$2MgCl_2(l\ or g)+SiO_2(s)+O_2(g)\ \rightarrow\ Mg_2SiO_4(s)+2Cl_2(g):\Delta G^{\circ}_{[Eq.\ (7)]}=-79\ \text{kJ at 1000 °C} \quad (7)$$

As can be seen in Fig. 10(b), both the MgO and Mg_2SiO_4 particles were simultaneously observed in the C50 composite.

In the hot corrosion by Na_2SO_4, both the idiomorphic MgO and forsterite particles were observed irrespective of the sample compositions (Fig. 11). This slightly different result from that obtained in case of NaCl attack may be due to a somewhat different situation that only the cordierite phase was severely attacked by Na_2SO_4 at 1000 °C. To consider the formation mechanism of both idiomorphic particles on the corroded surfaces, similar reaction processes to those described in NaCl attack, which should require the transportation of some kind of the Mg-related species to the outmost surface, could be applied for Na_2SO_4 attack. Under corrosive Na_2SO_4 environment in a crucible, the cordierite component directly reacted with molten Na_2SO_4 to produce $MgSO_4$ or MgO according to the following reactions. [The formation of Na_2O was not favorable because the free energy change of the reaction $Na_2SO_4(l)\ \rightarrow\ Na_2O(s)+SO_2(g)+1/2O_2(g)$ is + 349 kj/mol at 1000 °C.]

$$Mg_2Al_4Si_5O_{18}(s)+2Na_2SO_4(l)\ \rightarrow\ 4NaAlSiO_4(s)+SiO_2(s)+2MgSO_4(s) \quad (8)$$

$$Mg_2Al_4Si_5O_{18}(s)+2Na_2SO_4(l)\ \rightarrow\ 4NaAlSiO_4(s)+SiO_2(s)+2MgO(s)+SO2(g)+O_2(g) \quad (9)$$

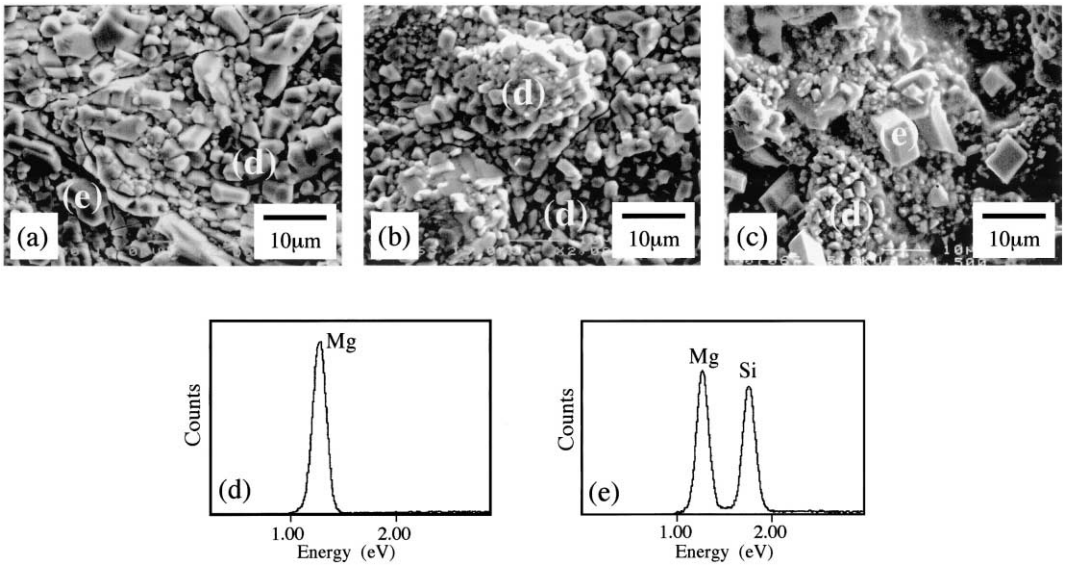

Fig. 11. Surface morphologies of (a) C80, (b) C50, (c) C20 composites corroded by Na_2SO_4 with EDS results of (d), (e) particles.

The free energy change of the former reaction was estimated to be −463 kJ and the latter −190 kJ at 1000 °C, indicating that both reactions were thermodynamically favored under the present conditions. As shown in the phase diagram of the Na_2SO_4–$MgSO_4$ system,[22] solid $MgSO_4$ can melt in molten Na_2SO_4 to form homogeneous liquid at 1000 °C. Therefore, the upward diffusion of the $MgSO_4$ species through liquid phase would be possible during hot corrosion. On the outmost surface, the following reactions might take place:

$$MgSO_4(l) \rightarrow MgO(s) + SO_2(g) + 1/2O_2(g) : \Delta G^{\circ}_{[\text{Eq. (10)}]} = +3 \text{ kJ at } 1000\ ^{\circ}\text{C} \quad (10)$$

$$2MgSO_4(l) + SiO_2(s) \rightarrow Mg_2SiO_4(s) + 2SO_2(g) + O_2(g) : \Delta G^{\circ}_{[\text{Eq. (11)}]} = -55 \text{ kJ at } 1000\ ^{\circ}\text{C} \quad (11)$$

If the corrosion by Na_2SO_4 was dominated by the reaction (9), the diffusion process of the MgO species up to the outer surface, which was similar to that described in case of NaCl attack, was necessarily required. Because the solubility of MgO in molten Na_2SO_4 is also very small (0.013 mol.%) at 1000 °C, it was unlikely that the MgO species formed by the reaction (9) was transported as soluble species through molten Na_2SO_4.

From the above discussion, Eqs. (5) and (8) may be the fundamental chemical reaction occurring at corrosion front in case of NaCl and Na_2SO_4 attack, respectively.

4. Conclusions

Cordierite/mullite (C/M) composites with the C:M molar ratios of 8:2 (C80), 5:5 (C50) and 2:8 (C20) were fabricated from the corresponding mixtures of silica and alumina sols and $Mg(OH)_2$ powder. Sintered composites were then heated at 1000 °C for 24 h in the concentrated NaCl and Na_2SO_4 atmospheres. For all the composites corroded in this study, a characteristic Mg distribution in which an extending Mg-deficient inner region followed a Mg-enriched surface layer was observed. In the hot corrosion by NaCl, nepheline and carnegieite were detected as the predominant corrosion products for the C80 and C20 composites, respectively. The cross-sectional X-ray elemental analysis and microstructural observation with SEM showed that the corroded layers consisted of two distinct regions where both cordierite and mullite were chemically attacked near the surface part and only the cordierite phase was damaged in the succeeding inner one. On the contrary, the corrosive Na_2SO_4 preferably attacked the cordierite component in the C/M composites, resulting in the formation of nepheline as the corrosion product for any compositions. Thus, in the C/M composites, the mullite component showed a better corrosion resistance against NaCl and Na_2SO_4 than cordierite at 1000 °C in air.

Acknowledgements

This study was partly supported by the Japan Society for the Promotion of Science, Grant-in-Aid for Scientific Research (B), No. 12450348, 2000.

References

1. Bianco, R. and Jacobson, N., Corrosion of cordierite ceramics by sodium sulphate at 1000 °C. *J. Mater. Sci.*, 1989, **24**, 2903–2910.
2. Higashi, K. and Maeno, H., The latest status of the development of the advanced ceramic tube filter. *Reports Res. Lab. Asahi Glass Co., Ltd*, 1992, **42**(1), 81–95.
3. Alvin, M. A., Lippert, T. E. and Lane, J. E., Assessment of porous ceramic materials for hot gas filtration applications. *Ceram. Bull.*, 1991, **70**(9), 1491–1498.

4. Mussler, B. H. and Shafer, M. W., Preparation and properties of mullite-cordierite composites. *Am. Ceram. Soc. Bull.*, 1984, **63**, 705–714.
5. Ikawa, H., Watanabe, T., Urabe, K. and Udagawa, S., Thermal expansion and microstructure of cordierite and mullite composite. *J. Ceram. Soc. Jpn.*, 1985, **93**, 762–767 (in Japanese)..
6. Rasch, H., Considering some thermal applications for cordierite and cordierite-mullite materials. *Ceram. Forum Int./Ber. DKG*, 1987, **64**, 454–458.
7. Monroe, D. L., Wachtman, J. B. Jr. and Gault, C., The mechanical properties of cordierite–mullite composites as a function of temperature. In *Euro-Ceramics, 3: Engineering ceramics (Proceedings of the First European Ceramic Society Conference)*, ed. G. de With *et al*. Elsevier Science Publishing, London, 1989, pp. 3.394–3.408.
8. Anderson, R. M., Gerhardt, R., Wachtman, J. B. Jr., Onn, D. and Beecher, S., Thermal, mechanical, and dielectric properties of mullite-cordierite composites. In *Advances in Ceramics, 26; Ceramic Substrates and Packages for Electronic Applications (Proceedings of the International Symposium on Ceramic Substrates and Packages)*, ed. M. F. Yan *et al*. The American Ceramic Society, Westerville, 1989, pp. 265–277.
9. Hodge, J. D., Microstructure development in mullite-cordierite ceramics. *J. Am. Ceram. Soc.*, 1989, **72**, 1295–1298.
10. Takahashi, J., Kawai, Y. and Shimada, S., Hot corrosion of cordierite ceramics by Na- and K-salts. *J. Euro. Ceram. Soc.*, 1998, **18**, 1121–1129.
11. Farris, R. E. and Allen, J. E., Aluminous refractoriesalkali reactions. *Iron Steel Eng.*, 1973, **50**(2), 67–74.
12. Kennedy, C. R., Alkali attack on a mullite refractory in the grand forks energy technology center slagging gasifier. *J. Mater. Energy Syst.*, 1981, **3**, 27–31.
13. Rigby, G. R. and Hutton, R., Action of alkali and alkali-vanadium oxide slags on alumina-silica refractories. *J. Am. Ceram. Soc.*, 1962, **45**(2), 68–73.
14. Jacobson, N. S., Lee, K. N. and Yoshio, T., Corrosion of mullite by molten salts. *J Am Ceram Soc*, 1996, **79**(8), 2161–2167.
15. Schairer, J. F. and Bowen, N. L., The system Na_2O–Al_2O_3–SiO_2. *Am. J. Sci.*, 1956, **254**, 129–195.
16. Okawara, S. and Yamaguchi, A., Corrosion of mullite refractory by alkaline vapor. *Yogyo-Kyokai-Shi*, 1969, **77**(6), 208–216 (in Japanese).
17. Babushkin, V. I., Matveyev, G. M. and Mchedlov-Peyrossyan, O. P., *Thermodynamics of Silicates*. Springer-Verlag, New York, 1985, 399–423.
18. Chase, M. W. Jr. (ed.), *NIST-JANAF Thermochemical Tables*. J. Phys. Chem. Ref. Data Monograph No. 9 (Part I and II). Am. Chem. Soc. and Am. Inst. Phys., Washington DC, 1998.
19. *Phase Diagrams for Ceramists*. Am Ceram Soc, Columbus, 1964.
20. Sata, T. *et al*., *Advances in Ceramics*, vol. 10, ed. W. D. Kingery. Am. Ceram. Soc., Columbus, 1985, pp. 541.
21. Janz, G. J., ed., *Molten Salts Handbook*. Academic Press, New York, 1967 pp. 180.
22. *Phase Diagrams for Ceramists*. Am Ceram Soc, Columbus, 1964.